

DOI: 10.1002/cssc.201402865

New Benzo[1,2-*b*:4,5-*b'*]dithiophene-Based Small Molecules Containing Alkoxyphenyl Side Chains for High Efficiency Solution-Processed Organic Solar Cells

Zhengkun Du,^[a, b] Weichao Chen,^[a] Shuguang Wen,^[a] Shanlin Qiao,^[a] Qian Liu,^[a] Dan Ouyang,^[a, b] Ning Wang,^[a] Xichang Bao,^[a] and Renqiang Yang^{*,[a, c]}

A new acceptor–donor–acceptor (A–D–A) small molecule, namely, BDT-PO-DPP, based on the alkoxyphenyl (PO)-substituted benzo[1,2-*b*:4,5-*b'*]dithiophene (BDT) derivative and the diketopyrrolopyrrole (DPP) unit was synthesized as an electron donor for solution-processed small-molecule organic solar cells (SMOSCs). BDT-PO-DPP exhibited good thermal stability, with a 5% weight-lost temperature at 401 °C under a nitrogen atmosphere. BDT-PO-DPP exhibited a lower HOMO energy level of –5.25 eV and a weaker aggregation ability than alkoxy-substituted BDT-O-DPP. A bulk heterojunction SMOSC device

based on BDT-PO-DPP and [6,6]-phenyl-C₆₁-butyric acid methyl ester was prepared, and it showed a power conversion efficiency up to 5.63% with a high open-circuit voltage of 0.83 V, a short circuit current density of 11.23 mAcm⁻², and a fill factor of 60.37% by using 1,2-dichlorobenzene as the co-solvent after thermal annealing at 110 °C. The results indicate that the alkoxyphenyl-substituted BDT derivative is a promising electron-donor building block for constructing highly efficient solution-processed SMOSCs.

Introduction

Recently, bulk heterojunction (BHJ) organic solar cells (OSCs) have attracted considerable attention because of their prominent advantages, which include easy fabrication, light weight, low cost, and large area fabrication on flexible substrates.^[1–8] Currently, solution-processed BHJ solar cells based on conjugated polymers as donors (D) and fullerene derivatives as acceptors (A) have been widely studied, and promising power conversion efficiencies (PCEs) of over 9% have been achieved.^[9] In contrast, solution-processed small-molecule organic solar cells (SMOSCs) have not been studied so intensively.^[10–17] Relative to their polymeric counterparts, SMOSCs show better prospects of industrialization, including monodispersity, a well-defined chemical structure, synthetic reproducibility, and easy purification. Although the PCEs of solution-processed SMOSCs

have recently been increased up to 6–8%, the development of novel D–A small molecules is still significant for the commercial application of SMOSCs in the future.^[12,15]

To achieve high-performance SMOSCs, low band gap small molecule containing alternating D and A units in the backbone or side chains have been widely designed and synthesized because of the easily tunable energy levels and solubility.^[18–20] In the past few years, considerable attention has been paid to benzo[1,2-*b*:4,5-*b'*]dithiophene (BDT) derivatives.^[11,15,20] The BDT unit has a symmetric and coplanar conjugated structure, and most importantly, it can be relatively easily modified and it exhibits good electron delocalization and excellent hole mobility. BDT-based derivatives have proven to be excellent donor materials in OSCs.^[21–23] Chen and co-workers reported a 2D BDT-based small molecule, DR3TBDTT, that demonstrated a PCE as high as 8.12%.^[15] Their work also revealed that the nature of the acceptor end group mainly influences the performance of the resulting SMOSCs. Hence, to enhance light absorption and to tune the HOMO energy levels of small molecules, much effort has been devoted to the design of new acceptor building blocks. Among the vast variety of the developed electron-withdrawing groups, the diketopyrrolopyrrole (DPP) unit has recently attracted much attention in the design and synthesis of new polymers and small molecules for high-performance OSCs as a result of its strong light absorption in the visible light region and because of its good photochemical stability.^[14,19,24] Recently, Yao and co-workers reported three alkoxy- or alkylthienyl-substituted BDT derivative small molecules end capped by DPP as the donor.^[25] The resulting small molecules showed weaker aggregation ability and improved PCE values upon replacing the alkoxy chain by a alkylthienyl

[a] Z. Du,[†] Dr. W. Chen,[†] Dr. S. Wen, Dr. S. Qiao, Q. Liu, D. Ouyang, Dr. N. Wang, Dr. X. Bao, Prof. R. Yang
CAS Key Laboratory of Bio-based Materials
Qingdao Institute of Bioenergy and Bioprocess Technology
Chinese Academy of Sciences
Qingdao 266101 (PR China)
Fax: (+86) 532-80662778
E-mail: yangrq@qibebt.ac.cn

[b] Z. Du,[†] D. Ouyang
University of Chinese Academy of Sciences
Beijing 100049 (PR China)

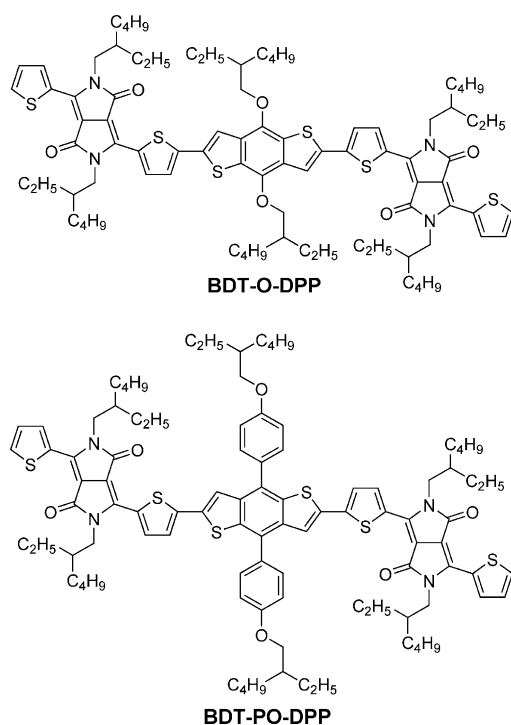
[c] Prof. R. Yang
State Key Laboratory of Luminescent Materials and Devices
South China University of Technology
Guangzhou 510641 (PR China)

[†] These authors contributed equally to this work.

 Supporting Information for this article is available on the WWW under <http://dx.doi.org/10.1002/cssc.201402865>.

group. In most cases, the PCEs of DPP-based SMOSCs are lower than 4%. However, Zhan and co-workers reported an alkylthienyl-substituted BDT-based small molecule, BDT-2DPP, that exhibited good photovoltaic performance with a PCE of 5.79%, and this is the highest value reported to date for SMOSCs based on DPP and BDT units.^[11] In comparison to alkylthienyl-substituted BDT, alkoxyphenyl-substituted BDT would be a promising 2D electron-donor material. Zou and co-workers reported an alkoxyphenyl-substituted BDT-based polymer (PBDTPO-DTBT) with a PCE of up to 6.2%.^[26]

In view of the above discussion, replacing the alkoxy side chain with an alkoxyphenyl group may be a good choice for improving the photovoltaic performance of BDT-based SMOSCs. This could increase the electronic delocalization and the torsion angle of the side chain, and it could also further improve thermal stability and reduce molecular self-aggregation. To our knowledge, alkoxyphenyl-substituted BDT-based small molecules have not been investigated for efficient SMOSCs. In this work, we designed and synthesized a novel small molecule, namely, BDT-PO-DPP (Scheme 1), with an al-



Scheme 1. Chemical structures of BDT-O-DPP and BDT-PO-DPP.

koxyphenyl (PO)-substituted BDT unit as the central electron donor and DPP units as the end-capped blocks. BDT-PO-DPP was found to exhibit excellent thermal stability and good solubility in common organic solvents. Finally, the relationship between the chemical structure and photovoltaic performance was investigated in detail. The film showed a hole mobility up to $2.98 \times 10^{-4} \text{ cm}^2 \text{ V}^{-1} \text{ s}^{-1}$ for BDT-PO-DPP, which was measured by the space-charge limit current (SCLC) model. The optimized OSCs based on BDT-PO-DPP as the donor and [6,6]-phenyl- C_{61} -butyric acid methyl ester (PC₆₁BM) as the acceptor showed

a high PCE of 5.63% with an open-circuit voltage (V_{oc}) of 0.83 V, a short-circuit current (J_{sc}) of 11.23 mA cm^{-2} , and a fill factor (FF) of 60.37% under the illumination of AM1.5 G (100 mW cm^{-2}).

Results and Discussion

Synthesis and characterization

For the design of BDT-PO-DPP, the BDT unit containing alkoxyphenyl side chains as the donor and the DPP unit as the acceptor were employed. Detailed synthetic routes to BDT-O-DPP and BDT-PO-DPP are outlined in Scheme 2. All reactions were performed under an argon atmosphere. Benzo[1,2-*b*:4,5-*b'*]dithiophene-4,8-dione, 2,6-bis(trimethyltin)-4,8-bis(2-ethylhexyloxy)benzo[1,2-*b*:4,5-*b'*]dithiophene (**5**), 1-bromo-4-(2-ethylhexyloxy)benzene (**2**), and 3-(5-bromothiophen-2-yl)-2,5-bis(2-ethylhexyl)-6-(thiophen-2-yl)pyrrolo[3,4-*c*]pyrrole-1,4(2*H*,5*H*)-dione (DPP-Br) were synthesized according to literature procedures. The target small molecule BDT-O-DPP was obtained in good yield by Stille coupling of **5** and **6** in the presence of catalytic amounts of tris(dibenzylideneacetone)dipalladium [$\text{Pd}_2(\text{dba})_3$] and tri(*o*-tolyl)phosphine [$\text{P}(o\text{-tol})_3$]. BDT-PO-DPP was synthesized by using the same coupling reaction of **4** and **6**. The chemical structures of related compounds were characterized by NMR spectroscopy, elemental analysis, mass spectrometry, and Fourier-transform infrared (FTIR) spectroscopy. The mass spectra were recorded with a Bruker Maxis UHR TOF spectrometer in the APCI mode. BDT-O-DPP and BDT-PO-DPP exhibited good solubility in common organic solvents, such as toluene, dichloromethane (CH_2Cl_2), chloroform (CHCl_3), and 1,2-dichlorobenzene (*o*-DCB).

Thermal stability

Thermogravimetric analysis (TGA) was used to investigate the thermal properties of BDT-O-DPP and BDT-PO-DPP. As shown in Figure 1, BDT-PO-DPP exhibits good thermal stability, with a 5% weight-lost temperature (T_d) at 401°C under a nitrogen atmosphere. Relative to that of BDT-O-DPP (361°C) and BDT-2DPP (388°C),^[11] the thermal stability of BDT-PO-DPP was improved owing to the introduction of the alkoxyphenyl side

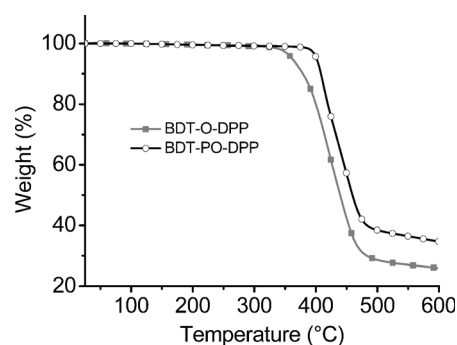
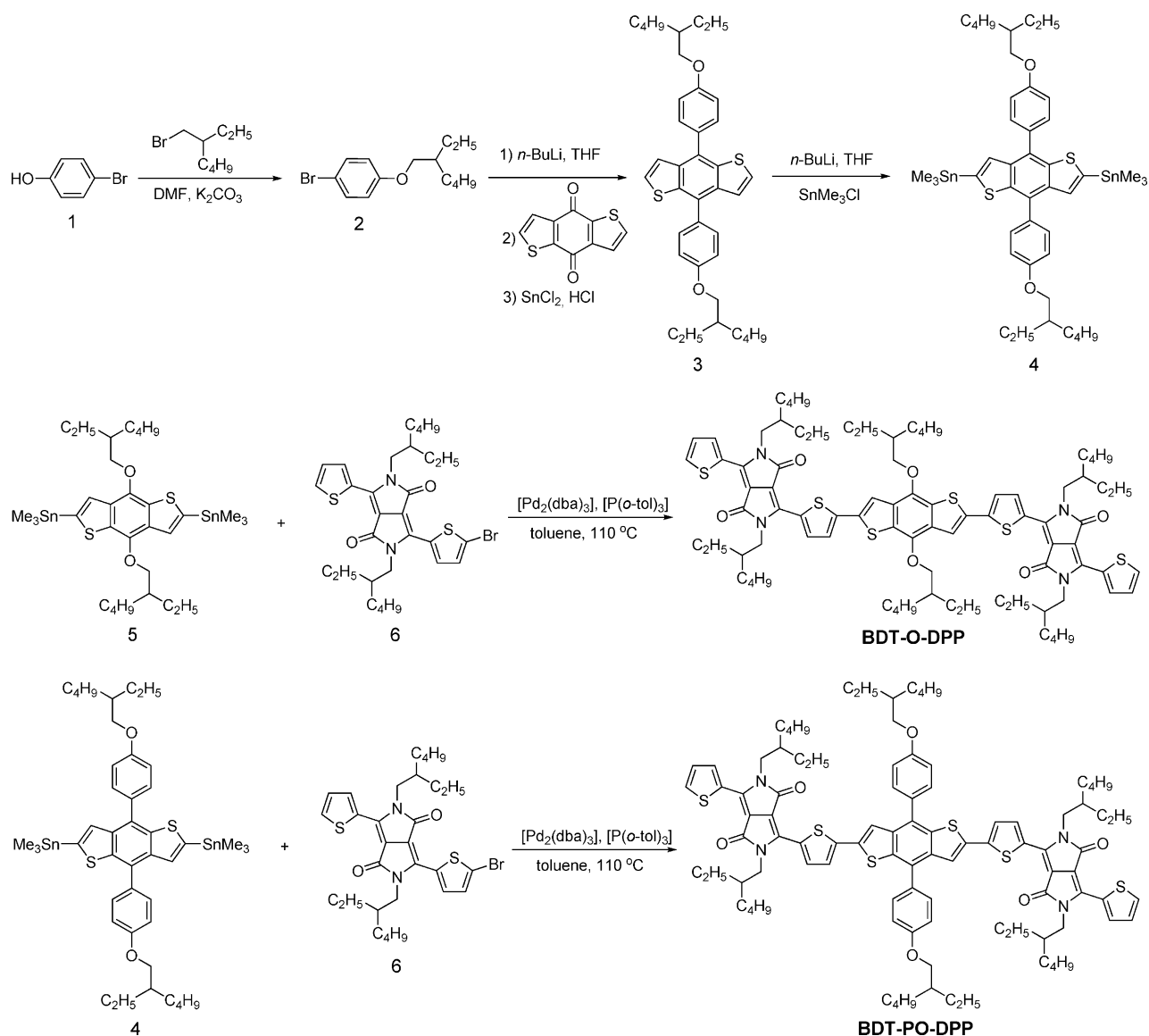


Figure 1. TGA curves of BDT-O-DPP and BDT-PO-DPP with a heating rate of $10^\circ\text{C min}^{-1}$ under a nitrogen atmosphere.



Scheme 2. Synthetic routes to BDT-O-DPP and BDT-PO-DPP.

chains. The high thermal stability of BDT-PO-DPP is adequate for application in solution-processed OSCs.

Optical properties

The normalized ultraviolet/visible (UV/Vis) absorption spectra of BDT-O-DPP and BDT-PO-DPP in dilute CHCl₃ solution (5 × 10⁻⁶ M) and as thin films are shown in Figure 2, and the data are summarized in Table 1. In CHCl₃ solution, BDT-O-DPP exhibits an absorption peak at λ = 622 nm. After replacing the alkoxy group with an alkoxyphenyl unit, the BDT-PO-DPP solution displays an absorption peak that is slightly redshifted to λ = 625 nm. As shown in Figure S1 (Supporting Information), the maximum molar extinction coefficient (ε_{max}) of BDT-PO-DPP (0.88 × 10⁵ L mol⁻¹ cm⁻¹ at λ = 625 nm) is lower than that of BDT-O-DPP (1.17 × 10⁵ L mol⁻¹ cm⁻¹ at λ = 622 nm) as a result of the decreased backbone planarity of BDT-PO-DPP. Relative to

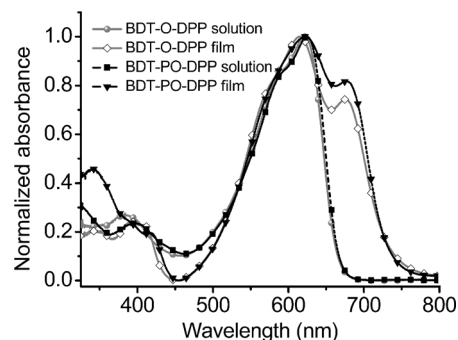


Figure 2. The normalized UV/Vis absorption spectra of BDT-O-DPP and BDT-PO-DPP in CHCl₃ solution and as thin films.

the absorptions in solution, as thin films both small molecules show absorptions that are remarkably redshifted and broader. In the long wavelength region, as-cast films of BDT-O-DPP and

Compound	λ_{abs} solution ^[a] [nm]	λ_{abs} film ^[b] [nm]	ΔE^{opt} ^[c] [eV]	E_{ox} ^[d] [V]	HOMO ^[e] [eV]	LUMO ^[f] [eV]
BDT-O-DPP	622	615, 675	1.69	0.75	-5.16	-3.47
BDT-PO-DPP	625	622, 677	1.70	0.84	-5.25	-3.55

[a] Measured in CHCl₃ solution. [b] Thin film spin coated from CHCl₃ solution onto ITO glass substrate. [c] Estimated from the absorption onset of the thin film. [d] Measured from the CV curves. [e] HOMO = -e(E_{ox} + 4.8 - 0.39). [f] Calculated from the difference between the HOMO and ΔE^{opt} .

BDT-PO-DPP show shoulder peaks at $\lambda = 675$ and 677 nm, respectively. However, the maximum absorption peak of the BDT-PO-DPP film is slightly redshifted (7 nm) relative to that of the BDT-O-DPP film, owing to alkoxyphenyl substitution. The broader absorption in the thin films originates from the formation of intermolecular aggregates in the solid state.^[11,15,26] Optical band gaps of BDT-O-DPP and BDT-PO-DPP calculated from the absorption edges of the thin films are approximately 1.69 and 1.70 eV, respectively.

Electrochemical properties

The electrochemical properties of BDT-O-DPP and BDT-PO-DPP were investigated by cyclic voltammetry (CV), and the corresponding data are summarized in Table 1. As shown in Figure 3, the oxidation onset potentials of BDT-O-DPP and BDT-PO-DPP are at approximately 0.75 and 0.84 V, respectively.

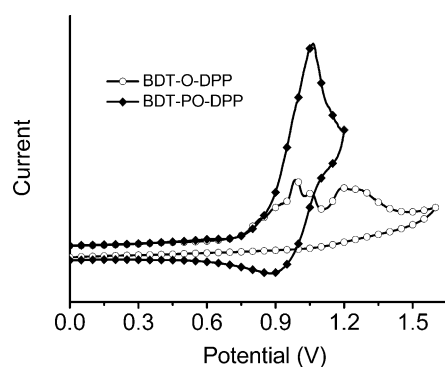


Figure 3. Cyclic voltammograms of BDT-O-DPP and BDT-PO-DPP films in 0.1 M nBu₄NPF₆/acetonitrile solution at a scan rate of 50 mVs⁻¹.

The corresponding HOMO levels of BDT-O-DPP and BDT-PO-DPP are -5.16 and -5.25 eV, respectively. By employing the empirical formula in Equation (1), the corresponding LUMO levels were calculated to be -3.47 eV for BDT-O-DPP and -3.55 eV for BDT-PO-DPP. From the CV results, one can observe that the energy levels of the small molecules could be well tuned by introducing different side chains on the molecular backbone. The downshift in the HOMO energy level of BDT-PO-DPP relative to that of BDT-O-DPP was mainly attributed to the weaker electron-donating ability of the alkoxyphenyl

group relative to that of the alkoxy group as a result of the larger torsion angle between the phenyl group and the backbone.^[27,28]

$$\text{LUMO} = \text{HOMO} + \Delta E^{\text{opt}} \quad (1)$$

The LUMO levels of the two target molecules are approximately 0.36 eV higher than that of the fullerene derivative acceptor PC₆₁BM, (-3.91 eV, Figure 4), which indicates that charge transfer from the small molecules to PC₆₁BM could be efficient.^[29-31]

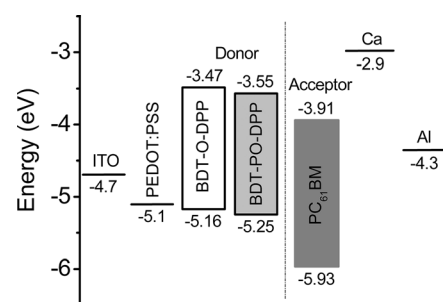


Figure 4. Diagram of the HOMO and LUMO energy levels of BDT-O-DPP and BDT-PO-DPP and other materials used in OSCs.

Theoretical studies

To better understand the effect of the side chains on the molecular optoelectronic properties, the electronic structures and geometries of BDT-O-DPP and BDT-PO-DPP were investigated by using density functional theory (DFT) calculations. All the alkyl side chains were replaced with methyl groups to reduce the computational cost. As shown in Figure 5, the torsion angle between the phenyl group and the backbone is approximately 58.6° for BDT-PO-DPP. As a result, BDT-O-DPP is slightly more planar than BDT-PO-DPP, which can be ascribed to steric hindrance in the phenyl side chain. This result indicates that the molecular conformation of BDT-PO-DPP could be finely

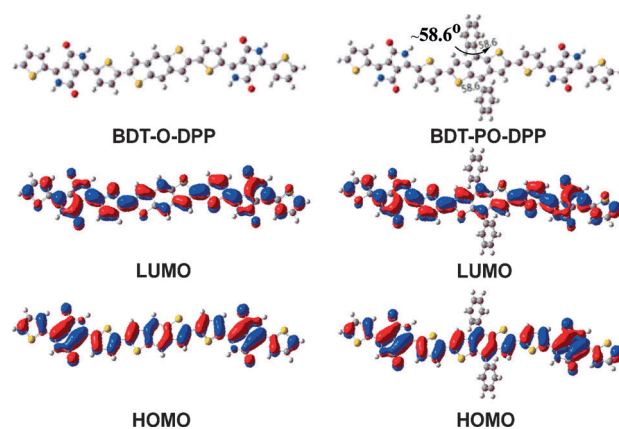


Figure 5. Optimized molecular geometries and frontier molecular orbitals of BDT-O-DPP and BDT-PO-DPP by using DFT calculations evaluated at the B3LYP/6-31G(d) level of theory. For clarity, all side chains are not shown.

tuned by introduction of an alkoxyphenyl group into the BDT central moiety. Although the molecular conformation is clearly different, the distribution state of the frontier molecular orbitals of BDT-O-DPP and BDT-PO-DPP are almost the same as that predicted by DFT calculations.

Photovoltaic properties

To investigate the photovoltaic performance of the two small molecules, a series of BHJ SMOSCs devices were fabricated with a typical configuration of ITO/PEDOT:PSS/small molecule:PC₆₁BM/Ca/Al [ITO=indium tin oxide, PEDOT:PSS=poly(3,4-ethylenedioxythiophene):poly(styrene sulfonate)]. The fabrication and measurements of the device are described in the Experimental Section. Detailed parameters of the device are summarized in Tables S1–S4 and Figures S2–S6.

The optimized device performance for both SMOSCs is shown in Table 2. For the BDT-O-DPP-based devices (Table S1), different weight ratios of BDT-O-DPP and PC₆₁BM (1.5:1, 1:1, and 1:1.5) were explored. With a decreasing D/A ratio in the active layer, the best device was obtained with BDT-O-DPP:PC₆₁BM at 1:1, which showed PCE=3.34%, V_{oc} =0.86 V, J_{sc} =9.02 mA cm⁻², and FF=42.97% without thermal annealing. If the D/A blend ratio was decreased to 1:1.5, the PCE of the device was clearly reduced to 2.49% owing to a reduction in the values of J_{sc} and FF (Figure S2). To further improve their photovoltaic properties, thermal annealing at different temperatures was employed. Upon increasing the temperature, the value of J_{sc} first increased and then decreased markedly. Upon thermal annealing at 110 °C, the device with a blend ratio of 1:1 showed the highest efficiency, with PCE=4.28%, V_{oc} =0.88 V, J_{sc} =9.54 mA cm⁻², and FF=51.15% (Figure S3).

For the BDT-PO-DPP-based SMOSCs without thermal annealing, upon decreasing the D/A ratio in the active layer from 1.5:1 to 1:1.5, the values of J_{sc} and FF for the devices first increased and then decreased slightly (Table S3). The best device was obtained with BDT-PO-DPP:PC₆₁BM in a 1:1 ratio, which showed PCE=3.53%, V_{oc} =0.80 V, J_{sc} =7.49 mA cm⁻², and FF=58.95%. If the D/A blend ratio was decreased to 1:1.5, the PCE of the device reduced noticeably to 2.97% owing to a reduction in the values of J_{sc} and FF. Upon thermal annealing at 110 °C, the device based on BDT-PO-DPP:PC₆₁BM (1:1 w/w) showed PCE=4.16%, V_{oc} =0.84 V, J_{sc} =8.22 mA cm⁻², and FF=60.30% (Figure S5). Otherwise, BDT-PO-DPP exhibited a FF value that was higher than that of BDT-O-DPP (60.30 vs. 51.15%); however, the value of V_{oc} decreased slightly from 0.88 to 0.84 V and the value of J_{sc} decreased from 9.54 to 8.22 mA cm⁻². Given the same device configuration, the variations in the values of V_{oc} and J_{sc} are likely associated with remarkable differences in the phase-separated nanostructures in the active layers.^[25] Interestingly, if *o*-DCB was added to the mixture solution as a co-solvent, the performance of the

Table 2. Photovoltaic performance of the BHJ small molecule OSCs under AM1.5 G conditions.

Donor/acceptor (w/w)	Annealing [°C]	V_{oc} [V]	J_{sc} [mA cm ⁻²]	FF [%]	PCE _{max} (PCE _{av} ^[c]) [%]
BDT-O-DPP:PC ₆₁ BM (1:1)	none	0.86	9.02	42.97	3.34 (3.16)
BDT-O-DPP:PC ₆₁ BM (1:1)	110 ^[a]	0.88	9.54	51.15	4.28 (4.07)
BDT-O-DPP:PC ₆₁ BM (1:1)	110 ^[a,b]	0.84	8.97	42.36	3.23 (3.08)
BDT-PO-DPP:PC ₆₁ BM (1:1)	none	0.80	7.49	58.95	3.53 (3.34)
BDT-PO-DPP:PC ₆₁ BM (1:1)	110 ^[a]	0.84	8.22	60.30	4.16 (3.98)
BDT-PO-DPP:PC ₆₁ BM (1:1)	110 ^[a,b]	0.83	11.23	60.37	5.63 (5.47)

[a] Thermal annealing at 110 °C for 10 min. [b] 1,2-Dichlorobenzene (3%) as the co-solvent. [c] The average PCE was obtained from ten devices.

device was further enhanced because of the improved miscibility of BDT-PO-DPP with PC₆₁BM and the decreased phase domain size. The optimized content of *o*-DCB was 3%. Following thermal annealing at 110 °C after spin coating, the device based on BDT-PO-DPP:PC₆₁BM (1:1 w/w) showed the highest PCE of 5.63% with V_{oc} =0.83 V, J_{sc} =11.23 mA cm⁻², and FF=60.37% (Figure S6).

The current density–voltage (J – V) curve of the device based on BDT-PO-DPP:PC₆₁BM (1:1 w/w) with the use of *o*-DCB as the co-solvent and thermal annealing at 110 °C and the corresponding external quantum efficiency (EQE) spectrum are shown in Figure 6. One can observe that the EQE of the optimized device covered a broad wavelength range from λ =325 to 750 nm. The maximum EQE plateau exceeded 50% from λ =550 to 700 nm. The EQE curve is consistent with its absorption spectrum as a thin film (Figure 2), and this indicates that the absorbed sunlight by the target small molecule could ef-

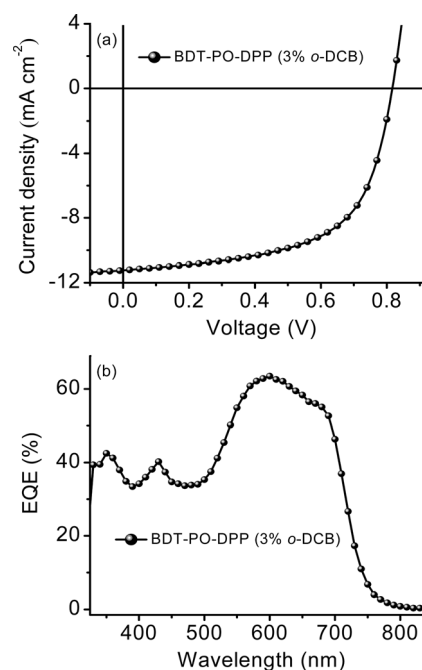


Figure 6. (a) J – V characteristic and (b) EQE spectrum of the device based on BDT-PO-DPP:PC₆₁BM (1:1 w/w) by using *o*-DCB as the co-solvent and thermal annealing at 110 °C.

fectively contribute to the generation of the photocurrent. The value of J_{sc} calculated from the EQE spectrum was 10.87 mA cm^{-2} , which is in accord with its photocurrent obtained from the J - V curve.

Hole mobility

The hole mobility is an important factor for OSCs, because of its direct influence on charge transport. High hole mobility could guarantee effective charge carrier transport to the electrodes and reduce the photocurrent loss in photovoltaic devices. The hole mobility of BDT-O-DPP and BDT-PO-DPP were measured by the SCLC method^[32–34] with a device structure of ITO/PEDOT:PSS/small molecule/Au. The SCLC is described by Equation (2):

$$J_{\text{SCLC}} = \frac{9}{8} \epsilon_0 \epsilon_r \mu_h \frac{V^2}{L^3} \quad (2)$$

in which J is the for current density, ϵ_0 is the permittivity of free space, ϵ_r is the relative dielectric constant of the transport medium, μ_h is the hole mobility, V is the internal potential in the device, and L is the thickness of the active layer. The internal potential V is obtained by subtracting the built-in voltage (V_{bi}) and the voltage drop (V_s) from the series resistance of the substrate from the applied voltage [V_{appl} , see Eq. (3)]:

$$V = V_{\text{appl}} - V_{bi} - V_s \quad (3)$$

As shown in Figure S6, according to Equation (2), the hole mobility was calculated to be 1.54×10^{-4} and $2.98 \times 10^{-4} \text{ cm}^2 \text{ V}^{-1} \text{ s}^{-1}$ for BDT-O-DPP and BDT-PO-DPP, respectively. Notably, the hole mobility of the BDT-PO-DPP film was higher than that of the BDT-O-DPP film under the same measurement conditions, which can be ascribed to the 2D conjugated structure of the BDT core.^[26]

X-ray diffraction

To elucidate the performance difference of BDT-O-DPP -and BDT-PO-DPP-based SMOSCs before and after thermal annealing at 110°C , the crystallinities of the BDT-O-DPP:PC₆₁BM film and BDT-PO-DPP:PC₆₁BM film were investigated by X-ray diffraction (XRD). As shown in Figure 7 a, the BDT-O-DPP:PC₆₁BM film exhibits an evident diffraction peak at $2\theta = 5.55^\circ$ corresponding to the (100) lattice plane of the molecule. Specifically, the second-order diffraction peak (200) and third-order diffraction peak (300) of the BDT-O-DPP:PC₆₁BM film with the use of *o*-DCB as the co-solvent are also clearly observed at $2\theta = 11.1^\circ$ and 16.5° , which is indicative of a continued increase in ordered arrangement after thermal annealing at 110°C . Additionally, the much narrower (100) diffraction peak of the annealed sample relative to that of the pristine sample also indicates that the crystalline size of the BDT-O-DPP:PC₆₁BM film grows significantly after thermal annealing at 110°C . The fact that the diffraction peak of the annealed film is stronger than that of the pristine sample reveals that the annealing process enhan-

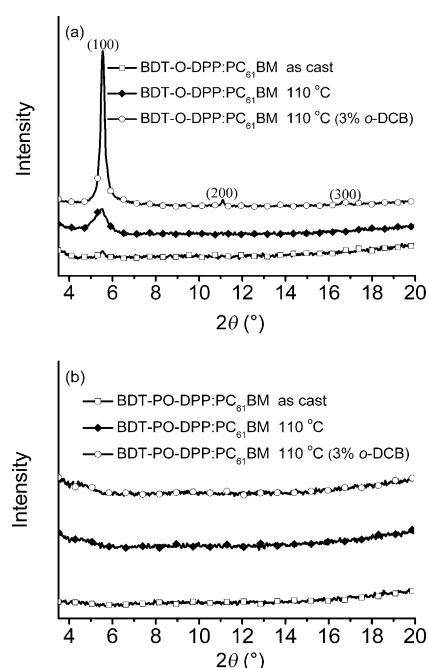


Figure 7. XRD patterns of (a) BDT-O-DPP:PC₆₁BM film and (b) BDT-PO-DPP:PC₆₁BM film spin coated from CHCl₃ solution before and after thermal annealing at 110°C .

ces the ordered aggregation of the BDT-O-DPP:PC₆₁BM blend in the donor phase.^[35,36] However, the film of the BDT-PO-DPP:PC₆₁BM blend does not show any noticeable diffraction peaks neither after thermal annealing nor after adding *o*-DCB as the co-solvent (Figure 7 b). Therefore, in comparison with BDT-O-DPP, the molecular aggregation of BDT-PO-DPP is drastically decreased, because of the introduction of large alkoxyphenyl side chains.

Morphology

To further understand the photovoltaic properties of the resulting small molecules, the morphologies of the blending films with a D/A ratio of 1:1 spin coated from their CHCl₃ solutions were recorded by tapping-mode atomic force microscopy (AFM). As shown in Figure 8, the pristine film of the BDT-O-DPP:PC₆₁BM blend shows a root-mean-square (RMS) roughness of 0.4 nm, and the film after thermal annealing exhibits a RMS roughness of 0.5 nm. Surprisingly, the surface roughness of the BDT-O-DPP:PC₆₁BM blend film with the use of *o*-DCB as the co-solvent significantly increased to 4.5 nm. The surface roughness of the BDT-O-DPP:PC₆₁BM blend film is well consistent with its aggregation ability, as discussed in the XRD section. The sharp increase in the surface roughness and the diffraction peak indicates that the active layer based on the BDT-O-DPP:PC₆₁BM blend could not form effective phase separation, and this led to a clear decrease in the value of J_{sc} . On the other hand, the film of the BDT-PO-DPP:PC₆₁BM blend shows RMS roughness values of 2.1 and 2.4 nm before and after thermal annealing at 110°C , respectively. Upon using *o*-DCB as the co-solvent, the film of the BDT-PO-DPP:PC₆₁BM blend shows

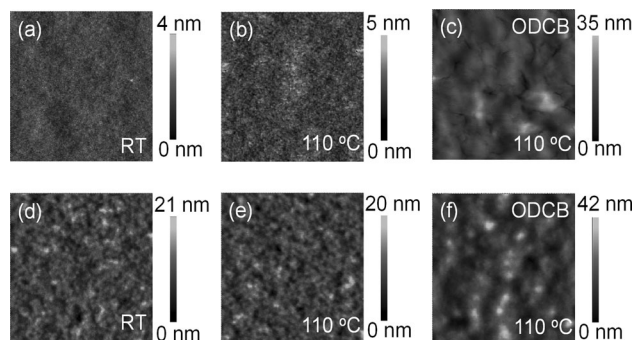


Figure 8. AFM height images of blend films of (a–c) BDT-O-DPP:PC₆₁BM and (d–f) BDT-PO-DPP:PC₆₁BM prepared by spin-coating from the CHCl₃ solution with a D/A ratio of 1:1.

a RMS roughness of 5.9 nm after thermal annealing at 110 °C. Although the RMS roughness becomes larger after thermal annealing, the miscibility of BDT-PO-DPP with PC₆₁BM improves. As shown in Figure 8c and f, the film of the BDT-PO-DPP:PC₆₁BM blend shows better phase separation than that of the BDT-O-DPP:PC₆₁BM blend film, which would decrease the trap state density existing in the boundary and therefore reduce the recombination current and improve the charge transport.^[37] This thereby increases the current density and the FF of BDT-PO-DPP-based SMOSCs in this work. Compared to BDT-PO-DPP, the domain size of BDT-O-DPP may overgrow,^[25] and this would result in a decrease in the donor–acceptor interface and the unbalanced charge transport, which would lead to relatively lower values of J_{sc} and FF.

Conclusions

A new donor (D)–acceptor (A) small molecule based on benzo[1,2-*b*:4,5-*b'*]dithiophene-containing alkoxyphenyl side chains, BDT-PO-DPP, was designed and synthesized. BDT-PO-DPP exhibited good thermal stability and a HOMO energy level of –5.25 eV. Through replacing the alkoxy chain by an alkoxyphenyl group, the resulting BDT-PO-DPP exhibited weaker aggregation ability than BDT-O-DPP. A bulk heterojunction small-molecule organic solar cell based on BDT-PO-DPP and PC₆₁BM was prepared, and it showed a PCE up to 5.63% with V_{oc} = 0.83 V, J_{sc} = 11.23 mA cm⁻², and FF = 60.37% upon using 1,2-dichlorobenzene as the co-solvent and thermal annealing at 110 °C. The results indicate that the alkoxyphenyl-substituted benzo[1,2-*b*:4,5-*b'*]dithiophene derivative is a promising electron-donor building block that can be used for the construction of high-efficiency solution-processed organic solar cells.

Experimental Section

Materials

[Pd₂(dba)₃], [P(*o*-tol)₃], *n*-butyllithium (*n*BuLi), trimethyltin chloride (SnMe₃Cl), and tin(II) chloride dihydrate (SnCl₂·2H₂O) were purchased from commercial sources and were used without further purification, unless otherwise mentioned. Toluene and THF were dried with sodium and were distilled before use. 1-Bromo-4-(2-eth-

ylhexyloxy)benzene (**2**), DPP-Br (**6**, Figure S8), and DPP were synthesized according to literature procedures.^[14,26,38] Synthetic routes to BDT-O-DPP and BDT-PO-DPP (Figure S8) are described below.

Syntheses

Compound 2: Under the protection of an argon atmosphere, 4-bromophenol (5.20 g, 30 mmol) and potassium carbonate (4.98 g, 36 mmol) were put into a two-necked flask, and then DMF (100 mL) was added. After stirring for 5 min, 2-ethylhexyl bromide (6.75 g, 35 mmol) was added by syringe. The mixture was heated to 120 °C for 24 h in the dark. The cooled mixture was poured into water and then extracted with ethyl ether (3×). The combined organic phase was dried with anhydrous MgSO₄. After removing the organic solvents, the residue was purified by silica gel column chromatography (petroleum ether). Compound **2** was obtained as a pale yellow oil (7.27 g, 85%). ¹H NMR (600 MHz, CDCl₃): δ = 7.36 (d, 2H), 6.78 (d, 2H), 3.80 (d, 2H), 1.70 (m, 1H), 1.51–1.28 (m, 8H), 0.93–0.89 ppm (m, 6H); ¹³C NMR (150 MHz, CDCl₃): δ = 158.52, 132.15, 116.34, 112.46, 70.78, 39.32, 30.49, 29.06, 23.83, 23.04, 14.08, 11.09 ppm.

Compound 3: In a 200 mL argon-purged flask, *n*BuLi (11.25 mL, 1.6 M in hexane) was added dropwise to a solution of compound **2** (5.13 g, 18 mmol) in THF (40 mL) at –78 °C. After the addition, the mixture was kept at this temperature for 1 h. Subsequently, benzo[1,2-*b*:4,5-*b'*]dithiophene-4,8-dione (1.32 g, 6.0 mmol) was added quickly, and the mixture was stirred for 2 h at 55 °C. After cooling down to room temperature, a solution of SnCl₂·2H₂O (10.83 g, 48.0 mmol) in 10% HCl (19.2 mL) was added, and then the mixture was stirred for an additional 2 h at 55 °C. The mixture was quenched with deionized water (50 mL) and extracted with ethyl ether. The combined organic extract was dried with anhydrous MgSO₄ and evaporated under vacuum. The raw compound was purified by a silica gel column chromatography (petroleum ether). Compound **3** was obtained as a white solid (1.43 g, 40%). ¹H NMR (600 MHz, CDCl₃): δ = 7.62 (d, 4H), 7.38 (d, 2H), 7.34 (d, 2H), 7.09 (d, 4H), 3.96 (d, 4H), 1.80 (m, 2H), 1.60–1.36 (br, 16H), 0.98 (t, 6H), 0.94 ppm (t, 6H); ¹³C NMR (150 MHz, CDCl₃): δ = 159.25, 138.30, 136.24, 131.41, 130.50, 130.01, 126.99, 123.09, 114.74, 70.57, 39.49, 30.61, 29.15, 23.94, 23.10, 14.13, 11.19 ppm; elemental analysis calcd (%) for C₃₈H₄₆O₂S₂ (598.90): C 76.21, H 7.74, O 5.34, S 10.71; found: C 76.29, H 7.81, S 10.80.

Compound 4: In a 100 mL argon-purged flask, *n*BuLi (3.25 mL, 1.6 M in hexane) was added to a solution of compound **3** (1.20 g, 2.0 mmol) in dry THF (40 mL) at 0 °C. After the addition, the mixture was kept at this temperature for 2 h, and then SnMe₃Cl (5.75 mL, 1.0 M in hexane) was added. Then, the mixture was stirred for 6 h at room temperature. Subsequently, the mixture was poured into deionized water (40 mL) and extracted with ethyl ether. The combined organic phase was dried with anhydrous MgSO₄. After removing the organic solvents, the residue was recrystallized from acetone to afford **4** as a pale yellow solid (1.07 g, 58%). ¹H NMR (600 MHz, CDCl₃): δ = 7.64 (d, 4H), 7.38 (s, 2H), 7.10 (d, 4H), 3.97 (d, 4H), 1.80 (m, 2H), 1.60–1.36 (br, 16H), 0.99 (t, 6H), 0.94 (t, 6H), 0.35 ppm (t, 18H); ¹³C NMR (150 MHz, CDCl₃): δ = 159.05, 142.59, 141.62, 137.07, 132.06, 130.86, 130.57, 128.45, 114.64, 70.49, 39.54, 30.63, 29.17, 23.96, 23.11, 14.14, 11.22, –8.36 ppm.

BDT-O-DPP: In a two-necked round-bottomed flask, compound **5** (0.23 g, 0.3 mmol) and compound **6** (0.37 g, 0.61 mmol) were dissolved in dry toluene (15 mL). After purging with argon for 25 min, [Pd₂(dba)₃] (14 mg) and [P(*o*-tol)₃] (27 mg) were added under the

protection of an argon atmosphere. The mixture was stirred and heated to reflux for 24 h. Then, the mixture was poured into deionized water (25 mL) and extracted with dichloromethane (3 × 25 mL). The combined organic phase was dried with anhydrous MgSO_4 and filtered. After removing the organic solvents, the raw product was purified by silica gel column chromatography (petroleum ether/ CH_2Cl_2) to give a blue-black solid (268 mg, 60%). ^1H NMR (600 MHz, CDCl_3): δ = 9.00 (d, 2H), 8.92 (d, 2H), 7.59 (d, 2H), 7.55 (s, 2H), 7.39 (d, 2H), 7.25 (t, 2H), 4.20 (d, 4H), 4.05 (m, 8H), 1.94 (m, 2H), 1.87 (m, 4H), 1.74 (m, 2H), 1.65 (m, 4H), 1.47–1.25 (m, 42H), 1.08 (t, 6H), 1.00–0.94 (m, 12H), 0.91–0.86 ppm (m, 18H); ^{13}C NMR (150 MHz, CDCl_3): δ = 161.65, 161.57, 144.44, 142.24, 140.17, 139.49, 136.78, 135.68, 135.42, 132.80, 130.56, 129.87, 129.49, 129.31, 128.45, 126.22, 117.58, 108.49, 108.16, 76.25, 45.97, 40.69, 39.31, 39.14, 30.45, 30.32, 30.31, 30.26, 30.23, 29.72, 29.25, 29.23, 28.46, 28.37, 23.86, 23.71, 23.57, 23.18, 23.11, 14.24, 14.09, 14.04, 11.36, 10.52, 10.29 ppm; MS (UHR-TOF): m/z : calcd. for $\text{C}_{86}\text{H}_{114}\text{N}_4\text{O}_6\text{S}_6$: 1490.7063 $[\text{M}]^+$; found: 1490.7057.

BDT-PO-DPP: Prepared by a procedure similar to that used to synthesize BDT-O-DPP starting from compound **4** (0.18 g, 0.20 mmol) and compound **6** (0.25 g, 0.41 mmol). Finally, a blue-black solid was obtained (0.21 g, 65%). M.p. 324.5 °C; ^1H NMR (600 MHz, CDCl_3): δ = 8.90 (d, 4H), 7.65 (d, 4H), 7.61 (d, 2H), 7.49 (s, 2H), 7.34 (d, 2H), 7.27 (d, 2H), 7.16 (d, 4H), 4.06–3.95 (m, 12H), 1.87–1.81 (m, 6H), 1.63–1.45 (m, 6H), 1.40–1.25 (m, 42H), 1.01 (t, 6H), 0.96 (t, 6H), 0.89–0.81 ppm (m, 24H); FTIR (KBr): $\tilde{\nu}$ = 3075.63, 2955.75, 2925.14, 2855.99, 1663.75, 1607.03, 1555.94, 1517.14, 1451.40, 1418.68, 1401.59, 1377.44, 1314.74, 1230.85, 1173.22, 1098.44, 1023.94, 856.65, 830.31, 809.76, 734.15, 702.84, 466.85 cm^{-1} ; MS (UHR-TOF): m/z : calcd. for $\text{C}_{98}\text{H}_{122}\text{N}_4\text{O}_6\text{S}_6$: 1642.7689 $[\text{M}]^+$; found: 1642.7683; elemental analysis calcd (%) for $\text{C}_{98}\text{H}_{122}\text{N}_4\text{O}_6\text{S}_6$ (1644.43): C 71.58, H 7.48, N 3.41, O 5.84, S 11.70; found: C 71.65, H 7.58, N 3.37, S 11.69.

Spectroscopic measurements

^1H NMR and ^{13}C NMR spectra were measured with a Bruker Avance III 600 spectrometer with tetramethylsilane (δ = 0 ppm) as an internal standard. UV/Vis absorption spectra were performed with a Hitachi U-4100 spectrophotometer. TGA was performed with a TA Q600 thermogravimetric analyzer. Cyclic voltammetry (CV) measurements were taken with a CHI660D electrochemical workstation. CV experiments were performed at room temperature with a conventional three-electrode system by using a platinum wire as the counter electrode, a saturated calomel electrode (SCE) as the reference electrode, and a glassy carbon electrode as the working one. Tetrabutylammonium phosphorus hexafluoride (Bu_4NPF_6 , 0.1 M) in acetonitrile solution was used as the supporting electrolyte, and the scan rate was 50 mV s^{-1} . Ferrocene/ferrocenium (Fc/Fc^+) was used as the internal standard (the energy level of Fc/Fc^+ is -4.8 eV under vacuum), and the formal potential of Fc/Fc^+ was measured as 0.39 V vs. SCE. Elemental analysis was measured with a Vario EL Cube elemental analyzer. FTIR spectra were measured with a Nicolet iN10 infrared microscope.

Photovoltaic device fabrication and characterization

SMOSCs were fabricated with a structure of ITO/PEDOT:PSS/BDT-PO-DPP: $\text{PC}_{61}\text{BM}/\text{Ca}/\text{Al}$ by using the conventional solution spin-coating process. The ITO-coated glass substrates were cleaned by ultrasonic treatment in detergent, deionized water, acetone, and isopropyl alcohol for 20 min. A layer of PEDOT:PSS was spin coated

(4000 rpm, ≈ 40 nm thick) onto the ITO glass. After baking at 150 °C for 25 min, the substrates were transferred into a glove box. Subsequently, the active layer was spin coated from different ratio blends of BDT-PO-DPP (or BDT-O-DPP) and PC_{61}BM in CHCl_3 solution at 1500 rpm for 25 s on the ITO/PEDOT:PSS substrate. Finally, a 10 nm Ca layer and a 100 nm Al layer were successively deposited onto the active layer under high vacuum by a shadow mask to define the area of 0.1 cm^2 ($< 3 \times 10^{-4}$ Pa). Thermal annealing was performed by placing the completed devices on a digitally controlled hotplate at different temperatures in a nitrogen-filled glove box.

The structure of the film was evaluated by grazing incidence X-ray diffraction (GIXRD, Bruker D8 Advance). Surface morphological characterizations of the films were performed by tapping-mode atomic force microscopy (AFM, Agilent 5400). Current density–voltage (J – V) characteristics of the devices were measured with a Keithley 2420 source measurement unit under simulated 100 mW cm^{-2} (AM1.5 G) irradiation from a Newport solar simulator. Light intensity was calibrated with a standard silicon solar cell. The external quantum efficiencies (EQEs) of the solar cells were analyzed by using a certified Newport incident photon conversion efficiency (IPCE) measurement system.

Acknowledgements

This work was supported by the Ministry of Science and Technology of China (2014CB643501, 2010DFA52310), the National Natural Science Foundation of China (21202181, 21204097, 51173199, 61107090, and 61405209), Chinese Academy of Sciences (KGCX2-YW-399 + 9–2), and Qingdao Municipal Science and Technology Program (11–2–4–22-hz).

Keywords: donor–acceptor systems • energy conversion • organic solar cells • small molecules • thin films

- [1] G. Yu, J. Gao, J. C. Hummelen, F. Wudl, A. J. Heeger, *Science* **1995**, *270*, 1789–1791.
- [2] B. C. Thompson, J. M. Frechet, *Angew. Chem. Int. Ed.* **2008**, *47*, 58–77; *Angew. Chem.* **2008**, *120*, 62–82.
- [3] J. Chen, Y. Cao, *Acc. Chem. Res.* **2009**, *42*, 1709–1718.
- [4] X. Guo, M. Baumgarten, K. Müllen, *Prog. Polym. Sci.* **2013**, *38*, 1832–1908.
- [5] J. Hou, H. Y. Chen, S. Zhang, R. I. Chen, Y. Yang, Y. Wu, G. Li, *J. Am. Chem. Soc.* **2009**, *131*, 15586–15587.
- [6] B. Walker, C. Kim, T.-Q. Nguyen, *Chem. Mater.* **2011**, *23*, 470–482.
- [7] E. Bundgaard, O. Hagemann, M. Manceau, M. Jørgensen, F. C. Krebs, *Macromolecules* **2010**, *43*, 8115–8120.
- [8] D. Demeter, T. Rousseau, P. Leriche, T. Cauchy, R. Po, J. Roncail, *Adv. Funct. Mater.* **2011**, *21*, 4379–4387.
- [9] Z. He, C. Zhong, S. Su, M. Xu, H. Wu, Y. Cao, *Nat. Photonics* **2012**, *6*, 591–595.
- [10] H. Choi, H. M. Ko, N. Cho, K. Song, J. K. Lee, J. Ko, *ChemSusChem* **2012**, *5*, 2045–2052.
- [11] Y. Lin, L. Ma, Y. Li, Y. Liu, D. Zhu, X. Zhan, *Adv. Energy Mater.* **2013**, *3*, 1166–1170.
- [12] D. H. Wang, A. K. K. Kyaw, V. Gupta, G. C. Bazan, A. J. Heeger, *Adv. Energy Mater.* **2013**, *3*, 1161–1165.
- [13] T. Bura, N. Leclerc, R. Bechara, P. Lévêque, T. Heiser, R. Ziessel, *Adv. Energy Mater.* **2013**, *3*, 1118–1124.
- [14] S. Loser, C. J. Bruns, H. Miyachi, R. P. Ortiz, A. Facchetti, S. I. Stupp, T. J. Marks, *J. Am. Chem. Soc.* **2011**, *133*, 8142–8145.
- [15] J. Zhou, Y. Zuo, X. Wan, G. Long, Q. Zhang, W. Ni, Y. Liu, Z. Li, G. He, C. Li, B. Kan, M. Li, Y. Chen, *J. Am. Chem. Soc.* **2013**, *135*, 8484–8487.

- [16] A. B. Tamayo, X. D. Dang, B. Walker, J. Seo, T. Kent, T. Q. Nguyen, *Appl. Phys. Lett.* **2009**, *94*, 103301.
- [17] Y. Chen, X. Wan, G. Long, *Acc. Chem. Res.* **2013**, *46*, 2645–2655.
- [18] Y. Sun, G. C. Welch, W. L. Leong, C. J. Takacs, G. C. Bazan, A. J. Heeger, *Nat. Mater.* **2012**, *11*, 44–48.
- [19] J. Liu, Y. Sun, P. Moonsin, M. Kuik, C. M. Proctor, J. Lin, B. B. Hsu, V. Promarak, A. J. Heeger, T.-Q. Nguyen, *Adv. Mater.* **2013**, *25*, 5898–5903.
- [20] D. Patra, T.-Y. Huang, C.-C. Chiang, R. O. V. Maturana, C.-W. Pao, K.-C. Ho, K.-H. Wei, C.-W. Chu, *ACS Appl. Mater. Interfaces* **2013**, *5*, 9494–9500.
- [21] L. Dou, J. Gao, E. Richard, J. You, C. C. Chen, K. C. Cha, Y. He, G. Li, Y. Yang, *J. Am. Chem. Soc.* **2012**, *134*, 10071–10079.
- [22] J. Min, Z. G. Zhang, S. Zhang, Y. Li, *Chem. Mater.* **2012**, *24*, 3247–3254.
- [23] W. Li, W. S. Roelofs, M. M. Wienk, R. A. Janssen, *J. Am. Chem. Soc.* **2012**, *134*, 13787–13795.
- [24] W. Li, K. H. Hendriks, A. Furlan, W. S. C. Roelofs, S. C. J. Meskers, M. M. Wienk, R. A. J. Janssen, *Adv. Mater.* **2014**, *26*, 1565–1570.
- [25] J. Huang, X. Wang, X. Zhang, Z. Niu, Z. Lu, B. Jiang, Y. Sun, C. Zhan, J. Yao, *ACS Appl. Mater. Interfaces* **2014**, *6*, 3853–3862.
- [26] J. Yuan, L. Xiao, B. Liu, Y. Li, Y. He, C. Pan, Y. Zou, *J. Mater. Chem. A* **2013**, *1*, 10639–10645.
- [27] L. Huo, J. Hou, S. Zhang, H. Y. Chen, Y. Yang, *Angew. Chem. Int. Ed.* **2010**, *49*, 1500–1503; *Angew. Chem.* **2010**, *122*, 1542–1545.
- [28] A. Gadisa, M. Svensson, M. R. Andersson, O. Inganäs, *Appl. Phys. Lett.* **2004**, *84*, 1609–1611.
- [29] M. C. Scharber, D. Mühlbacher, M. Koppe, P. Denk, C. Waldauf, A. J. Heeger, C. J. Brabec, *Adv. Mater.* **2006**, *18*, 789–794.
- [30] C. J. Brabec, C. Winder, N. S. Sariciftci, J. C. Hummelen, A. Dhanabalan, P. A. van Hal, R. A. J. Janssen, *Adv. Funct. Mater.* **2002**, *12*, 709–712.
- [31] Y. Chen, Z. Du, W. Chen, Q. Liu, L. Sun, M. Sun, R. Yang, *Org. Electron.* **2014**, *15*, 405–413.
- [32] A. G. G. Malliaras, J. R. Salem, P. J. Brock, C. Scott, *Phys. Rev. B* **1998**, *58*, 13411–13414.
- [33] V. D. Mihailetschi, J. Wildeman, P. M. W. Blom, *Phys. Rev. Lett.* **2005**, *94*, 126602.
- [34] X. Hu, L. Zuo, W. Fu, T. T. Larsen-Olsen, M. Helgesen, E. Bundgaard, O. Hagemann, M. Shi, F. C. Krebs, H. Chen, *J. Mater. Chem.* **2012**, *22*, 15710–15716.
- [35] U. Zhokhavets, T. Erb, G. Gobsch, M. Al-Ibrahim, O. Ambacher, *Chem. Phys. Lett.* **2006**, *418*, 347–350.
- [36] G. Wei, S. Wang, K. Sun, M. E. Thompson, S. R. Forrest, *Adv. Energy Mater.* **2011**, *1*, 184–187.
- [37] Z. Bao, A. J. Lovinger, A. Dodabalapur, *Appl. Phys. Lett.* **1996**, *69*, 3066–3068.
- [38] O. P. Lee, A. T. Yiu, P. M. Beaujuge, C. H. Woo, T. W. Holcombe, J. E. Millstone, J. D. Douglas, M. S. Chen, J. M. J. Fréchet, *Adv. Mater.* **2011**, *23*, 5359–5363.

Received: August 20, 2014

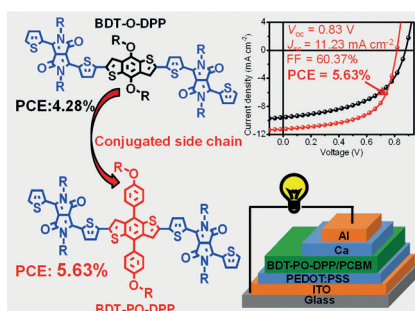
Published online on ■ ■ ■ ■, 0000

FULL PAPERS

Z. Du, W. Chen, S. Wen, S. Qiao, Q. Liu,
D. Ouyang, N. Wang, X. Bao, R. Yang*



New Benzo[1,2-*b*:4,5-*b'*]dithiophene-Based Small Molecules Containing Alkoxyphenyl Side Chains for High Efficiency Solution-Processed Organic Solar Cells



Taking it up a notch: A 2D small molecule based on the benzo[1,2-*b*:4,5-*b'*]dithiophene (BDT) unit containing alkoxyphenyl (PO) side chains is synthesized for organic solar cells. By replacing the alkoxy side chain with an alkoxyphenyl group, the molecular aggregation of BDT-PO-DPP is effectively reduced. A small-molecule organic solar cell based on BDT-PO-DPP/PC₆₁BM exhibits promising power conversion efficiency. DPP = diketopyrrolopyrrole.